Mechanism and Machine Theory 78 (2014) 116–130

Contents lists available at ScienceDirect

Mechanism and Machine Theory

journal homepage: www.elsevier.com/locate/mechmt

Towards an underactuated finger exoskeleton: An optimization process of a two-phalange device based on kinetostatic analysis

Alessandro Battezzato *

Center for Space Human Robotics@Polito, Istituto Italiano di Tecnologia, Corso Trento 21, 10129 Turin, Italy

ARTICLE INFO

Article history:
Received 16 September 2013
Received in revised form 13 March 2014
Accepted 15 March 2014
Available online 12 April 2014

Keywords:
Hand exoskeleton
Underactuation
Kinetostatics
Optimization
EVA

ABSTRACT

The current paper deals with the kinetostatic analysis and consequent optimization of an underactuated mechanism, whose aim is to constitute an exoskeleton device, designed to enhance the force of the human finger with whom it is coupled. Given an exoskeleton architecture, optimal from the point of view of the simplicity, the geometric parameters are further optimized, to let the transmitted forces be as similar as possible to the specific force profile, set as a reference for the device. In particular, extra-vehicular activity (EVA) for astronauts is recognized as a possible field for hand exoskeletons, since EVA gloves are very demanding in terms of strength and fatigue. Thus, the force profile for a specific EVA glove is provided as an example, and different optimized devices are obtained from the stochastic optimization process. Their kinetostatic performances are hence analyzed and discussed, thanks to a properly defined performance index. Finally, a verification of the actual encumbrance of the synthesized structure is performed, with respect to EVA-specific constraints.

1. Introduction

In the recent years hand exoskeletons, used to empower the human user or to assist him during medical rehabilitation, have become a research field that conveys a lot of interest. As a consequence, many prototypes have been presented in the past years [1]. However, since the human hand is a very complex mechanism, with at least 24 DOFs (degrees of freedom) [2], then the task of coupling it with an external actuated device is very difficult. In general, not all the DOFs of the hand are reproduced (like the abduction/adduction of the fingers) or they are kept passive, as their range of motion is negligible with respect to the flexion/extension movement [3]. Moreover, to reduce the complexity and the number of actuators, some fingers can be coupled together [4]. When dealing with a single finger mechanism, to reduce complexity and weight, i.e., the number of actuators, the simplest solution would be to mechanically link the consecutive flexion/extension DOFs [4,5]. For example, in the human hand the rotation angle of the second phalange and the third one are dependent on each other, according to a physiological law that sets the ratio between the two. Moreover, considering a "typical" grasping configuration, a similar ratio can be established between the first and the second phalange angles [6]. However, a similarly conceived mechanism does not allow the flexibility that such a mechanism would require when worn by a human user, as it practically has a single DOF. Another possible philosophy would be to maintain the multi-DOF finger mechanism, but reducing the number of actuators.

The aim of the current paper is to explore this possibility, referred to as underactuation, which has been deeply investigated for robotic hands [7,8] as well as prosthetic devices [9]. In fact, as can be found in literature, a number of robotic hands or fingers

* Tel.: +39 0110903414.
E-mail address: alessandro.battezzato@iit.it.

http://dx.doi.org/10.1016/j.mechmachtheory.2014.03.007
0094-114X/

have been designed and prototypes have been built and tested [10–14]. However, a similarly inspired design for what concerns hand exoskeletons is much rarer. Specific needs and requirements can be attributed to this application field. In detail, the fact of reducing the number of actuators, i.e. the weight and bulk of the system, are particularly valuable factors, as an exoskeleton has to be worn and therefore an excessive complication and weight affects negatively the dexterity and fatigue of the user. Some examples of underactuated exoskeletons are present in literature: usually, they drive the fingertip, leaving the human finger to adjust its configuration accordingly [15,16]. Also Chiri et al. [3,17] have proposed an underactuated mechanism, but their design is not very efficient, since the actuators have to work against springs whose preload has to be high to make the joints stiffer.

As a first step, this paper identifies a basic underactuated mechanism for a finger exoskeleton. In order to maintain the weight and complexity as low as possible, an only two-phalange mechanism is considered: it is a quite common solution for exoskeletons [4,18–20]. As will be shown, the mechanism, which descends from existing fingers for underactuated robotic hands [21,22], can be proposed as a valid and compact solution for an exoskeleton, with some necessary modifications. Then, the geometry of the system is investigated, as well as the kinetostatic analysis. The latter permits one to identify the behavior of the system along the workspace, identifying the capability of the device to transmit actual forces to the human phalanges [23]. At this point, an optimization of the geometric parameters of the system can be done, in order to make the force transmission to the human finger have a desired shape and trend. A specific case study will be proposed: the development of an exoskeleton to overcome the hand fatigue of astronauts during EVA (extra-vehicular activity). In fact, pressurized EVA gloves have been identified as a very demanding task, and they constitute an ideal field of application for hand exoskeletons, whose aim is to empower human users [24–26]. The optimization of the device, as it involves several parameters in a non-linear problem, is performed through a stochastic algorithm, namely the simulated annealing one [27], that will be briefly introduced and explained. An index, used to characterize the performance of each solution, is defined. Finally, the output solutions of the optimized architecture will be shown, in order to establish if they are able to perform some typical tasks of EVA, given their effective bulk over the finger.

Each finger of the human hand is composed of three phalanges, linked with one another by revolute joints, and appears as a serial kinematic chain, as shown in Fig. 1. The metacarpus, considered fixed, is connected to the first phalange through a metacarpophalangeal abduction/adduction joint (MCP_{aa}), and a consequent flexion/extension joint (MCP_{fe}). Then, other two flexion/extension joints are present, that link the other two phalanges: the proximal interphalangeal (PIP) and the distal interphalangeal (DIP). However, when conceiving a finger exoskeleton, usually the MCP_{aa} joint is neglected, or kept passive, as its range of motion is negligible with respect to the other joints. Moreover, according to the grade of simplicity that the system needs, one or even two of the more distal phalanges can be eliminated from the system. In the current paper, a kinematic structure equivalent to a 2-DOF serial chain is proposed, taking into account the MCP_{fe} and the PIP joints. It is a compromise solution, that, as will be underlined later, is the most suitable architecture for the practical application that will be proposed in the following sections.

When dealing with robotic hands, the kinematics of each finger can be reproduced mimicking the human hand, as the biomechanical axes can be easily reproduced through mechanical revolute joints. However, the design of a finger exoskeleton is much more demanding, as any interference between the device and the finger itself has to be avoided. As the biomechanical joint axes are now inside the finger, two solutions are possible for the exoskeleton: on the first side, mechanical revolute joints, whose axes coincide with the biomechanical ones, placed laterally with respect to the finger. On the other side, remote mechanisms, usually placed over the finger and which realize a virtual joint in correspondence of the actual biomechanical one. If the former solution is simpler, it is not suitable for the MCP joint and it exploits the space among the fingers, which is very narrow and easily leads to lack of comfort. The latter, even if more complex, as it has several joints, fits perfectly the human finger kinematics. Both the described philosophies obtain a device that autonomously reproduces the finger kinematics; in fact, it is also possible to conceive a simplified mechanism that exploits the finger itself to realize, for example, a four-bar mechanism [28]. However, this strategy has not been considered in the current paper, since it has the drawback of not allowing high loads to be transmitted to the finger, as the human joints should sustain high reaction forces.

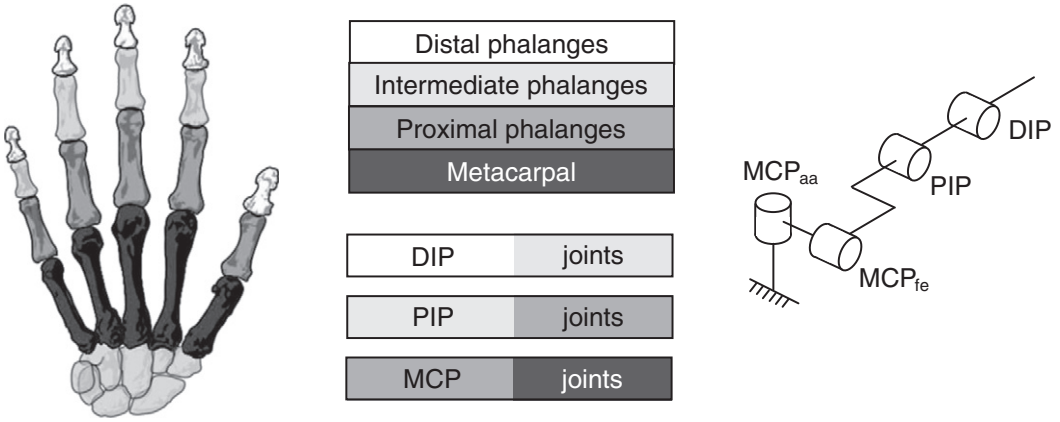

Fig. 1. Human finger kinematic scheme.

A solution based on a remote mechanism that realizes virtual joints, inspired by Zong et al. [29], is here considered. As stated in [5], the double-parallelogram remote structure here proposed is the best compromise among the complexity of implementation, and bulk and mechanical characteristics, and is therefore ideal for a finger exoskeleton.

A 3D virtual reconstruction of the actual prototype of the exoskeleton is shown in Fig. 2, as well as the kinematic principle adopted for the remote center joint. Even if the actual structure is not immediate, it is kinematically equivalent to a plain two-DOF serial chain, and at this stage it is not important if these two axes are real or virtual.

As a consequence, in the following Sections the double-parallelogram mechanisms will be neglected, and they will be represented as a 2-DOF serial chain, whose revolute joints coincide with the virtual ones, as it can be seen in Fig. 3.

If the mechanism shown in Fig. 3 reproduces the same kinematics of the human finger and can be referred to as the finger-like part, then it is necessary to design also a transmission part, coupled with the former one, that transmits the actuation force and realizes the underactuation principle. Probably, the simplest structure that can be employed to actuate the finger-like part is a 2-bar mechanism, connected to the second phalange through a revolute hinge. Usually, the choice of underactuation requires the presence of springs and limit stops, as can be seen in Fig. 4. These elements prevent the exoskeleton from assuming undesired configurations, and they limit the range of motion of the phalanges. Moreover, the spring prevents the mechanism from collapsing or having uncontrolled motion, due to its own weight and inertial forces. The presence of the limit stops also permits to give a proper preload to the springs (as can be seen in the first configuration of Fig. 4). Then, the application of the actuation torque to the transmission part lets the mechanism rotate until the first phalange touches the corresponding finger phalange. However, at this stage the presence of the spring lets the finger-like mechanism act as a rigid body. When the contact is established, the whole mechanism becomes a four-bar linkage and the second phalange of the finger-like part rotates until it touches the corresponding finger phalange. The spring now works against the actuator: hence, its stiffness and preload parameters have to be kept as low as possible.

2. Kinetostatic analysis of the mechanism

As said before, the finger exoskeleton mechanism is composed of the finger-like part, namely segments O_1O_2 and O_2O_3, and the transmission part, that includes elements *AB* and *BC*, according to the notation of Fig. 5. The whole structure is bi-dimensional and constitutes a closed-loop one, as points O_1 and A both lie on the ground. The finger-like part exchanges forces with the external world, while the actuation is placed on the rotational axis located at point A, applying a torque on the *AB* bar. A number of reference systems and rotation angles are set to describe the position of the mechanism. A coordinate system x_0y_0 is placed at point O_1, and it also sets a reference horizontal direction, necessary to define many rotation angles. The coordinate system x_1y_1 is linked to the bar O_1O_2, obtained from the system x_0y_0 through a θ_1 rotation. Similarly, a θ_2 rotation angle leads to the coordinate system x_2y_2, linked to the O_2O_3 bar. The rotation of the bar *AB* with respect to the x_0 direction is identified by the θ_A angle, while the θ_B angle quantifies the rotation of the bar *BC*. Moreover, an angle θ_c between the segments *AB* and *BC*, is introduced; it is $\theta_c = \pi - \theta_A - \theta_B$ Some vectors are also defined, useful to write the position equations: the generic position vector of a point J with respect to the center K of an L reference system is ${}^L p_{KJ}$, while its module is l_{KJ} In particular, the position vector of C with respect to O_2 is ${}^2 p_{O_2C} = \begin{bmatrix} l_{O_2Cx} & l_{O_2Cy} \end{bmatrix}^T$.

The closed-loop position equation of the structure is:

$$p_{O_1O_2} + p_{O_2C} - p_{O_1A} = p_{AB} + p_{BC}. \tag{1}$$

Eq. (1) is the basis of the position analysis of the structure. If the angles θ_1 and θ_2 that are coupled with a human finger, are known, then the first member of Eq. (1) is known, the position of point C is univocal and the other angles can be determined:

$$\theta_C = \operatorname{acos} \frac{l_{AB}^2 + l_{BC}^2 - l_{AC}^2}{2 l_{AB} l_{BC}}. \tag{2}$$

Then, it is:

$$\theta_A = \pi - \theta_C - \operatorname{acos} \frac{l_{AC}^2 + l_{BC}^2 - l_{AB}^2}{2 l_{AC} l_{BC}} + \operatorname{atan} \frac{l_{ACy}}{l_{ACx}} \tag{3}$$

where ${}^0 p_{O_2C} = \begin{bmatrix} l_{O_2Cx} & l_{O_2Cy} \end{bmatrix}^T$ is the left side of Eq. (1), and l_{AC} is its magnitude. In order to determine the behavior of the mechanism and the possibility of applying forces to the human finger, a quasi-static modeling of the system is done. The force actions applied to the system are represented in Fig. 6. The methodology presented here is basically taken from [23], where the kinetostatic analysis is applied to a generic underactuated finger with *n* DOFs. The first step consists of equating the input and the output virtual powers; then it is:

$$k^T \omega_i = f^T v_f \tag{4}$$

where $k = [T_a - k_s \Delta\theta_2]^T$ is the input torque exerted by the actuator and the spring (acting on point O_2), whose rotational stiffness is k_s, $\omega_i = \begin{bmatrix} \dot{\theta}_A & \dot{\theta}_2 \end{bmatrix}^T$ is the corresponding angular velocity vector, f is the vector of the contact wrenches, and v_f expresses

the twist of the corresponding contact points. The generic wrench is $f = [\bar{\zeta}_1 \quad \bar{\zeta}_2]^T$ where $\zeta_i = [f_{ix} \quad f_{iy} \quad \tau_i]^T$ ($\bar{\zeta}_i$ corresponds to ζ_i but poses the torque element before the force ones), and the twist is $v_f = [\xi_1 \quad \xi_2]^T$, where $\xi_i = [\omega_i \quad v_{ix} \quad v_{iy}]^T$ is the twist of the ith contact point D_i. A Jacobian matrix J can be found, that relates the twist with the rotational velocities of the phalanges, i.e. $v_f = J\omega_o$, where $\omega_o = [\dot{\theta}_1 \quad \dot{\theta}_2]^T$. Generally, the matrix J is not square: then, f is not unique for a given k and the system is indeterminate. In order to obtain a fully determinate system, the contact wrenches can be assumed to be pure forces normal to the respective phalanges, i.e. parallel to the local y axes. Hence, it is $\zeta_i = f_i j_i^*$ where f_i s the magnitude of the ith contact force and $j_i^* = [j_i^T \quad 0]^T$ is the unit wrench corresponding to a pure force along j_i, the unit vector along the local y_i axis of the phalange. The definition of f and v_f changes to $f = [f_1 \quad f_2]^T$ and $v_f = [\xi_1 \circ j_1^* \quad \xi_2 \circ j_2^*]^T$, where the operator $\circ$ stands for the reciprocal product of screws in the plane. It results in f containing the magnitude of the forces, while v_f is the vector of the projections of the contact twists onto the phalange normal directions. With this modification in mind, the J matrix is determined. The twist at the q-th contact point is:

$$\xi_q = \sum_{i=1}^{q} \dot{\theta}_i \xi_q^{O_i} \tag{5}$$

where $\xi_q^{O_i}$ is the joint twist of the q-th contact point associated with O_i. It is:

$$\xi_q^{O_i} = \begin{bmatrix} -1 \\ Qp_{O_iD_q} \end{bmatrix} \tag{6}$$

where the position vector $p_{O_iD_q}$ links the O_i origin point to the point of application of the force on the q-th phalange. The matrix Q derives from the representation of the cross product:

$$Q = \begin{bmatrix} 0 & 1 \\ -1 & 0 \end{bmatrix}. \tag{7}$$

Thus, the virtual power associated with the q-th contact point is:

$$\zeta_q \circ \xi_q = f_q j_q^* \circ \sum_{i=1}^{q} \dot{\theta}_i \xi_q^{O_i} = f_q \sum_{i=1}^{q} \dot{\theta}_i j_q^* \circ \xi_q^{O_i} = f_q \sum_{i=1}^{q} \dot{\theta}_i j_q{}^T Q p_{O_iD_q} = f_q \sum_{i=1}^{q} \dot{\theta}_i p_{O_iD_q}{}^T Q^T j_q = -f_q \sum_{i=1}^{q} \dot{\theta}_i p_{O_iD_q}{}^T i_q \tag{8}$$

where i_q is the unit vector that identifies the direction of the x_q axis. Thus, the J matrix is obtained; it has a lower triangular form:

$$J = \begin{bmatrix} -l_1 & 0 \\ -p_{O_1D_2}^T i_2 & -l_2 \end{bmatrix} \tag{9}$$

where $l_i = p_{O_iD_i}^T i_i$. Moreover, it is possible to define a relationship between the ω_i and the ω_o vectors, expressing the square of p_{BC} from Eq. (1); thus, it is:

$$l_{BC}^2 = p_{BC}^T p_{BC} = \left(p_{O_1O_2} + p_{O_2C} - p_{O_1A} - p_{AB}\right)^T \left(p_{O_1O_2} + p_{O_2C} - p_{O_1A} - p_{AB}\right). \tag{10}$$

Differentiating Eq. (10) with respect to time leads to the following matrix expression:

$$U\omega_o = T\omega_i \tag{11}$$

where:

$$U = \begin{bmatrix} p_{BC} \wedge p_{O_1C} & p_{BC} \wedge p_{O_2C} \\ 0 & 1 \end{bmatrix} \quad T = \begin{bmatrix} p_{AB} \wedge p_{BC} & 0 \\ 0 & 1 \end{bmatrix}. \tag{12}$$

Considering that $v_f = J\omega_o$ and inserting the results from Eq. (11) into Eq. (4) leads to:

$$f = J^{-T} U^T T^{-T} k. \tag{13}$$

As a first approximation, the spring placed at the O_2 revolute joint can be neglected, as its stiffness is maintained as low as possible, since the actuator has to work against it. Thus, only the first column of the matrix ($J^{-T}U^TT^{-T}$) is significant, as it expresses the transfer function f/T_a, i.e. the ratio between the forces at the contact points and the motor torque. In particular,

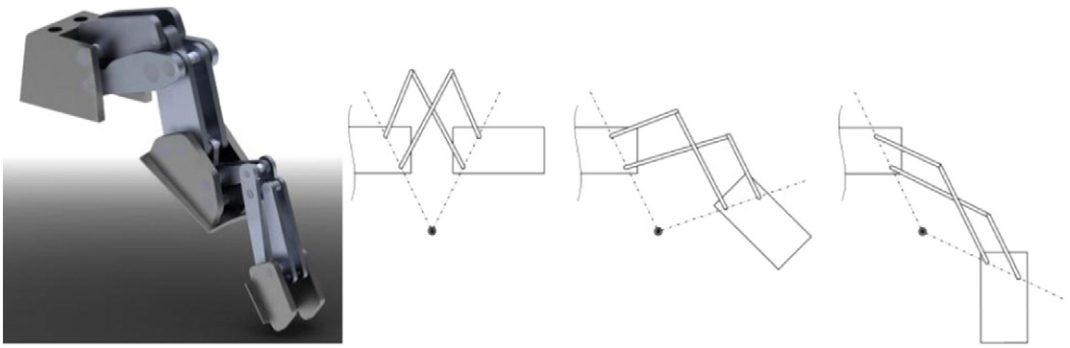

Fig. 2. Prototype of remote-center mechanism.

Eq. (13) requires two matrix inversions, regarding J and T. For what concerns J, the fact that it has a triangular form permits to calculate it in a simplified manner:

$$J^{-T} = \begin{bmatrix} -\frac{1}{l_1} & \frac{p_{O_1D_2}^T i_2}{l_1 l_2} \\ 0 & -\frac{1}{l_2} \end{bmatrix}. \tag{14}$$

On the other side, the inversion of T is feasible if and only if its determinant is not null. It descends that the system attains a singularity when the segments AB and BC are collinear. In particular, it corresponds to a Type I singularity, as defined in [30], as the system tends to lose a degree of freedom and reaches an extreme of its workspace. For example, another singularity configuration, which belongs to the Type II class, arises when p_{BC} and p_{O_2C} are collinear.

3. The optimization process

3.1. The EVA glove: illustrating a case study to understand a global approach

As said before, one of the main tasks that could be accomplished by a hand exoskeleton would be to empower the human user during demanding operations, that involve high loads and incipient fatigue of the subject. For example, astronauts performing EVA have to overcome the high stiffness of the pressurized spacesuit, that causes fatigue, pain and progressive lack of dexterity. This is particularly true for their hands, and a device that could decrease the effort of the subject to win the EVA glove stiffness would be particularly valuable [25]. Hence, a hand exoskeleton – or, as a first step, a finger exoskeleton – perfectly fits the needs of such application. In particular, the two-phalange finger exoskeleton investigated in the previous section is a design that takes into account the requirement of low bulk and weight (two phalanges instead of three) with the consideration that the third phalange is not very significant for a power grasping for astronauts wearing an EVA glove [4,31]. Moreover, given the fact that high loads are required to counterbalance the glove stiffness, a remote-center design, like the one illustrated in the previous sections, is now legitimized, in order to limit the reaction forces at the human finger joints.

Given the application for the exoskeleton, a preliminary definition of the target forces that the device should ideally exert on the human phalanges is necessary. These reference values are specified on the workspace as f_{REF_i}, where i stands for the ith

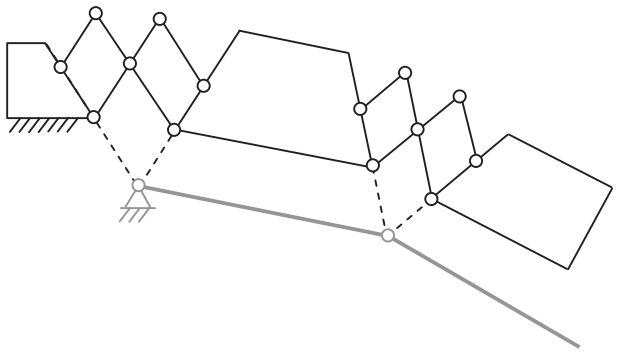

Fig. 3. Kinematic equivalence between the prototype mechanism and a 2-DOF serial chain.

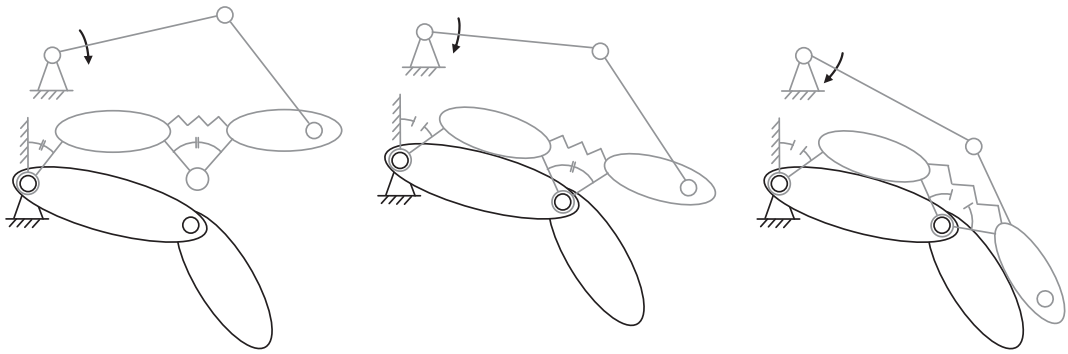

Fig. 4. Closure process of the underactuated mechanism.

phalange, and they constitute the basis for the definition of an objective function towards the optimization of the system. In practice, given the current EVA glove case, it is:

$$f_{REF\_i} = \varepsilon f_{GL\_i}. \tag{15}$$

The coefficient ε comprised of a value between 0 and 1, expresses the portion of the reaction force provided by the EVA glove's ith phalange f_{GL_i} to be effectively compensated. The $\varepsilon = 1$ case would ideally leave the user not feeling the presence of the glove: in practice, a lower value of the ε index will be chosen, in order to maintain force feedback to the user. At this point, it is necessary to define the law that expresses the load transmitted by the ith glove phalange along the workspace, i.e. $f_{GL\_i} = f_{GL\_i}(\theta_1, \theta_2)$. In the more general case, each glove phalange load depends on all the phalange angles, according to a non-linear trend. Different methodologies have been taken into account in the past to study the EVA glove stiffness: a possible strategy consists in an analytical reasoning, which involves the writing of a model of the glove, implementing the equilibrium equations of inflated rubber tubes and fabric tissues, validated through experimental tests [32]. Another approach, reported in [26], measures the flexion stiffness of each phalange of an existing EVA glove, in that case a Russian Orlan DM glove, through a specific test bench that relates the flexion angle to the corresponding reaction torque for each phalange. In the current case, the output equations of the second approach are taken into account. According to the results of [26], the reaction forces of the glove have a polynomial form with respect to the phalange angles; moreover, they depend on the level of pressurization of the EVA glove itself. The experimental coefficients of the polynomial laws expressing the relationship between the reaction forces and the phalange angles are reported in Appendix A.1. However, it has to be pointed out that even if the actual mechanical stiffness of the EVA glove were different (for example, considering a different model of EVA glove), the optimization approach here considered would remain valid. The only modification would be a different expression of the laws f_{GL_i}.

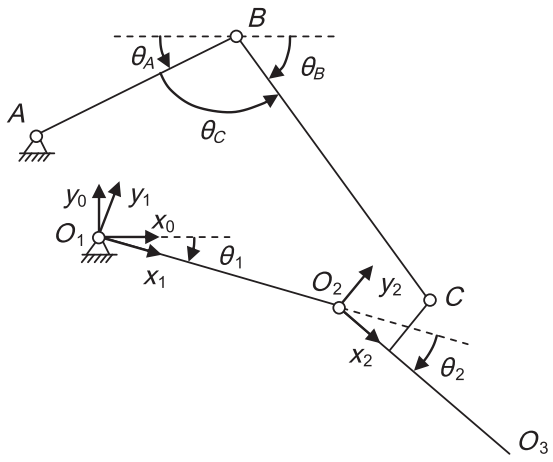

Fig. 5. Geometry of the finger exoskeleton.

In practice, if the two rows of Eq. (13) provide the variables f_1/T_a and f_2/T_a, then the optimization process will find the minimum of the function η_r, where the index r stands for 1, 2 or ∞, for the 1-norm, the 2-norm, and the ∞-norm, respectively. Hence it is:

$$\eta_r = \sum_{q=1}^{2}\left[\left|\left(\frac{f_q}{T_a}\right)T_{a_r} - f_{REF\_q}\right|\right]^r \text{ where } r = 1,2 \tag{16a}$$

$$\eta_\infty = \max\left[\left|\left(\frac{f_1}{T_a}\right)T_{a_\infty} - f_{REF\_1}\right|, \left|\left(\frac{f_2}{T_a}\right)T_{a_\infty} - f_{REF\_2}\right|\right]. \tag{16b}$$

If the 1-norm minimizes the mean value of the vector components, the ∞-norm minimizes the maximum value of the vector itself; finally, the 2-norm minimizes its magnitude. The problem delineated by the Eq. (16a) or (16b) is overdetermined, as a single variable T_{a_r} should ideally make the forces transmitted through the mechanism coincide with the reference ones. If the 1-norm and the ∞-norm do not have a closed form solution when dealing with overdetermined problems and they have to be found iteratively, the 2-norm, which is also referred to as the least squares solution, can be calculated as follows: given the generic $Ax = b$ problem, it is $x = A^I b$, where $A^I = (A^T A)^{-1} A^T$ is the left inverse of A. Applying this method – or equivalent ones, like the singular value decomposition, to find the pseudoinverse of the A matrix – leads to:

$$T_{a_2} = \frac{1}{\left(\frac{f_1}{T_a}\right)^2 + \left(\frac{f_2}{T_a}\right)^2}\left[\left(\frac{f_1}{T_a}\right)f_{REF\_1} + \left(\frac{f_2}{T_a}\right)f_{REF\_2}\right]. \tag{17}$$

Eq. (17) provides the actuation torque that gives the two transmitted forces f_1 and f_2 that get closer to f_{REF_1} and f_{REF_2} with respect to the 2-norm. Thus, inserting the value of T_{a_2} lets the function η_2 expressed by Eq. (16a) be minimized.

In practice, an indicator will be used to describe the performance of a geometrical solution for the underactuated mechanism. First of all, the whole workspace W will be investigated, i.e. along the defined range of θ_1 and θ_2 as the only acceptable solutions are the ones where f_1/T_a and f_2/T_a are real and positive. It means that the forces that the device transmits to the human finger are positive, i.e. the contact is guaranteed and the configuration of the underactuated mechanism is stable. Hence, a first optimization term consists in a binary-type function δ, whose values are null when the corresponding f_1/T_a or f_2/T_a are non-positive, unitary if and only if both are positive, i.e. the configuration is stable. The δ function also takes into account the fact of not passing through singularity branches, coherently limiting the effective workspace. Then, the function η_r will be evaluated along the workspace. As said before, this η_r index can be computed using different norms: the 2-norm will be exploited in the following, due to its computational advantages. A third function, that describes the weight that each configuration has on the global optimization process, is named as γ: it can assume any value between 0 (for configurations that have no influence on the final optimization) and 1 (for configurations that strongly affect the optimization process). Finally, a global performance index $\mathrm{GPI_r}$ can be calculated as:

$$\mathrm{GPI}_r = p_\eta f_\eta + p_\delta f_\delta \tag{18}$$

where:

$$f_\eta = \frac{\int_W \delta\eta_r \gamma dW}{\int_W \delta\gamma dW} \tag{19a}$$

$$f_\delta = \frac{\int_W (1-\delta)\gamma dW}{\int_W \gamma dW.} \tag{19b}$$

The p_η and p_δ coefficients balance the optimization trend towards the quality of the workspace, expressed through the η_r elated term, with respect to the spread of stable zones, or vice versa. The lower the index expressed in Eq. (18), the better the performance of the system.

Once that the strategy to evaluate mathematically each geometrical configuration has been established, then a suitable algorithm to find an optimized solution has to be used. Given the relatively high number of unknowns involved in the optimization process, then a stochastic algorithm is preferable. In fact, this kind of algorithm is not stuck by local minima and can easily handle non-linearities. Moreover, a well-designed algorithm is quite fast and effective in finding an optimal solution. To manage this problem, the SA (simulated annealing) logic has been chosen, thanks to its flexibility, ease of implementation and efficiency.

The SA method has been demonstrated to be effective in a wide range of optimization tasks. It mimics the annealing technique in metallurgy, where the heated material is progressively cooled in a controlled manner, in order to let the crystalline structure be more regular and defect-free, hence characterized by a state of minimum energy. In the initial phase, when the temperature is high, the atoms in the material can wander randomly, regardless of the level of internal energy of the system, that could even increase; then, the cooling process starts and the system tends towards situations where the internal energy is lower. In the algorithm proposed here, the concept of energy is linked to the previously defined performance index GPI_r: then, states of lower

energy correspond to geometric configurations more adherent to the reference distribution of forces. Given the initial step, the following iteration involves the creation of a geometric solution that is a neighbor of the previous one. The acceptance probability of this new configuration depends on two parameters: the internal energy levels of the parent and the neighbor configurations, referred to as $E_{(i)}$ and $E'_{(i)}$, and the value of the temperature parameter $T_{(i)}$. If there is a decrease in energy, i.e. $E'_{(i)} < E_{(i)}$, hence this neighbor configuration is accepted as the solution for the next iteration. If, on the other side, it is $E'_{(i)} > E_{(i)}$, then the acceptance probability of the neighbor solution is proportional to $exp\frac{E_{(i)}-E'_{(i)}}{T_{(i)}}$, whose form derives from the Boltzmann equation. This process, shown in Fig. 7, permits one to consider also solutions that temporarily worsen the $GPI_{2(i)}$ performance, saving the optimization from becoming stuck at local minima.

During the simulation, the temperature parameter $T_{(i)}$ progressively decreases: the trend of the ratio $T_{(i)}/T_{(0)}$, where $T_{(0)}$ is the temperature value at the beginning of the simulation, is reported in Fig. 7, too. This behavior lets the optimization process be greedier, hence slowly converging towards solutions with a lower value of internal energy, that is a low $GPI_{2(i)}$.

3.2. The EVA glove: the actual optimization output

The architecture introduced for the finger exoskeleton is defined through a number of geometric parameters, reported in Table 1: a first group includes some common fixed constants, while there are other two alternative sets of variable lengths that are allowed to vary within a specified range. The former, labeled as Set #1, individuates the range of variation of the geometric parameters that still permits one to perform one of the most important operations during EVA: using dedicated tools. A minimum offset between the tool handle and the surface of work is defined: it is equal to 7.6 cm, according to [33]. The latter, referred to as Set #2, constitutes a more stringent set of constraints for the variable parameters, as it permits an operation of grabbing a standard EVA handhold on the spaceship: a minimum offset of 5.75 cm is now posed as a requirement [33]. These values strongly affect not only the maximum values of l_{BC}, but also those of l_{O_2Cy}. Other elements that have been considered to delineate these ranges of variation are the fact that the points *B* and *C* should not go beyond the fingertip along the longitudinal direction of the finger; moreover, point *A* cannot interfere with the profile of the human hand. On the contrary, point *C* can be slightly lower with respect to such a profile, as it is more distal and hence there is lateral access to the finger, too.

In order to find a proper solution to the EVA glove problem, an optimization based on the GPI_2 function expressed through Eq. (18) is launched; it is performed through the SA stochastic algorithm, and the inequalities presented in Table 1 are the parameters object of the optimization itself.

The geometric configurations have been investigated along a 2-DOF workspace with $25° \le \theta_i \le 85°$, where $i = 1,2$. The lower boundary corresponds to a null force coming from the glove, i.e. it individuates the rest position of the glove. The upper one is lower than the range of motion of a barehanded subject, as stated in literature [31]. The reference forces f_{REF_1} and f_{REF_2} have been evaluated along such a workspace, given Eq. (15), Appendix A.1, and the coefficient $\varepsilon = 0.5$.

Given the previously described algorithm and the definition of GPI_2, a first choice of the optimization parameters is $p_\delta = 1e^3$ and $p_\eta = 1$, while the γ function is constantly unitary: it takes into account the extension of the workspace and not only its quality. Thus, the following optimized configuration, coming from the Set #1 constraints of Table 1, reported in Table 2, is obtained. The same table also presents the optimized solution in three different phases of an ideal grip: the initial condition with the finger in rest position ($\theta_1 = \theta_2 = 25°$) represented with solid lines, a mean configuration ($\theta_1 = \theta_2 = 55°$) with dashed lines, and the final one ($\theta_1 = \theta_2 = 85°$)with dotted lines. Then, the trend of the variables f_1 and f_2 are plotted, while T_{a_2} is also shown

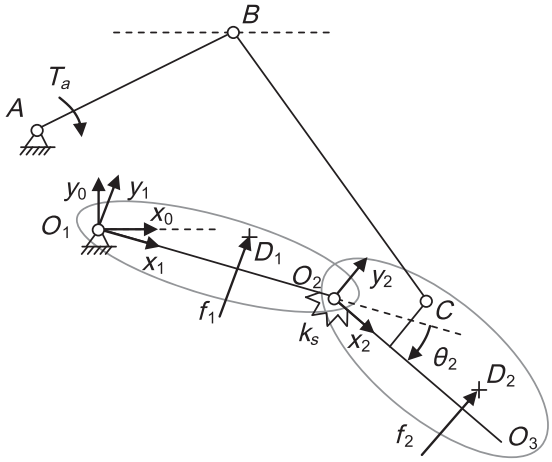

Fig. 6. Force actions applied to the finger exoskeleton.

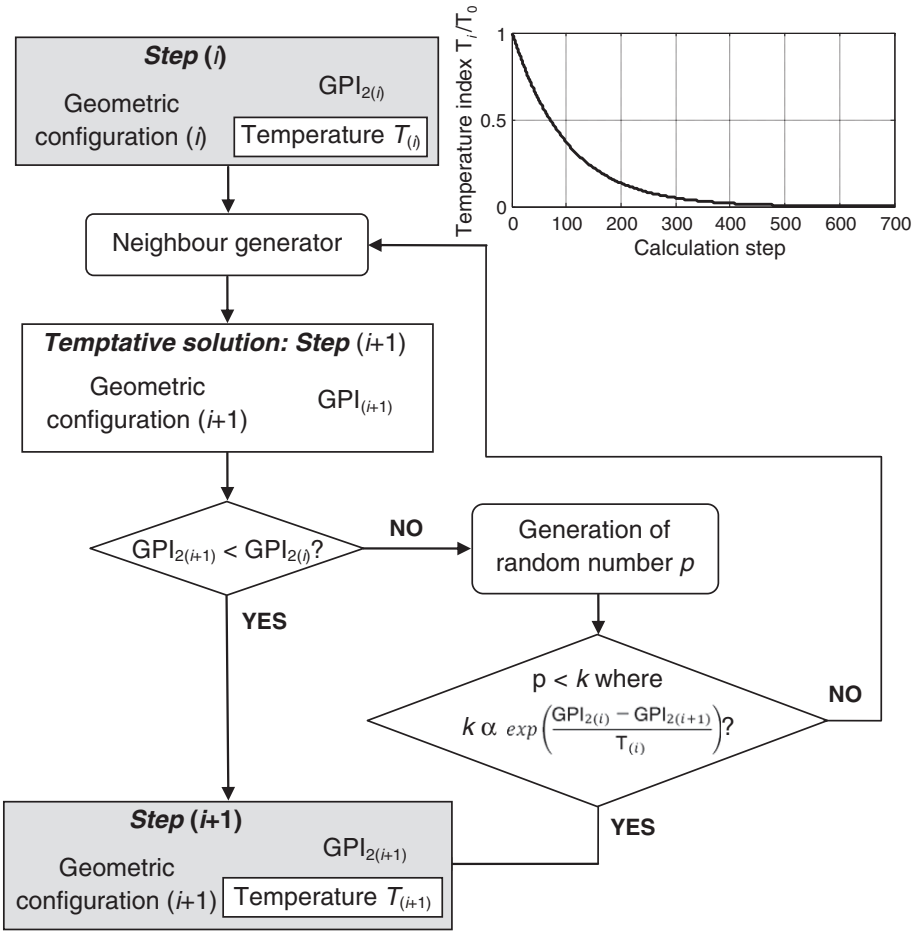

Fig. 7. Algorithm strategy: the simulated annealing case.

along the workspace, as it is calculated from Eq. (17). It is also significant to represent the mean value of the force f_{sub_i} that the human user has of exert along each phalange to win the stiffness of the corresponding glove phalanges. It is:

$$f_{sub_i} = f_{GL\_i} - f_i. \tag{20}$$

According to the choice of the coefficient $\varepsilon = 0.5$, a constant 50% quota should be applied directly by the subject; in practice, the human user contributions will be more widespread. Such contributions could also be negative: it means that the exoskeleton overcomes the reaction force of the glove, and the user also has to apply a force against the exoskeleton to reach an equilibrium (in practice, when grasping an object, the equilibrium would be guaranteed by higher contact forces between the glove and the object). In Table 2 there is also such a representation of the statistical distribution of the forces coming from the user along the portion of the workspace where the function δ is unitary: its mean value, as well as the maximum and minimum values of the human forces and their standard deviation are reported. These actual data are shown, marked by an *A*, along with the two opposite situations: the best case of constant 50% compensation (labeled by a *B*) and the absence of the exoskeleton device (that

Table 1
Geometrical constraints. Units are meters.

Fixed lengths	Set #1	Set #2
$l_{O_1O_2} = 0.050$	$-0.045 < l_{O_1Ax} < 0.028$	$-0.015 < l_{O_1Ax} < 0.028$
$l_{O_2O_3} = 0.025$	$0.016 < l_{O_1Ay} < 0.045$	$-0.015 < l_{O_1Ay} < 0.042$
$l_{O_1D_1x} = 0.040$	$0.03 < l_{AB} < 0.145$	$0.03 < l_{AB} < 0.12$
$l_{O_2D_2x} = 0.020$	$0.013 < l_{BC} < 0.050$	$0.012 < l_{BC} < 0.025$
	$-0.003 < l_{O_2Cx} < 0.0195$	$-0.003 < l_{O_2Cx} < 0.0195$
	$-0.01 < l_{O_2Cy} < 0.045$	$0.01 < l_{O_2Cy} < 0.030$

Table 2
Output of the simulation: Set #1 boundaries.

$p_\delta = 1e^3$ $p_\eta = 1$ $\gamma = 1_{cost}$	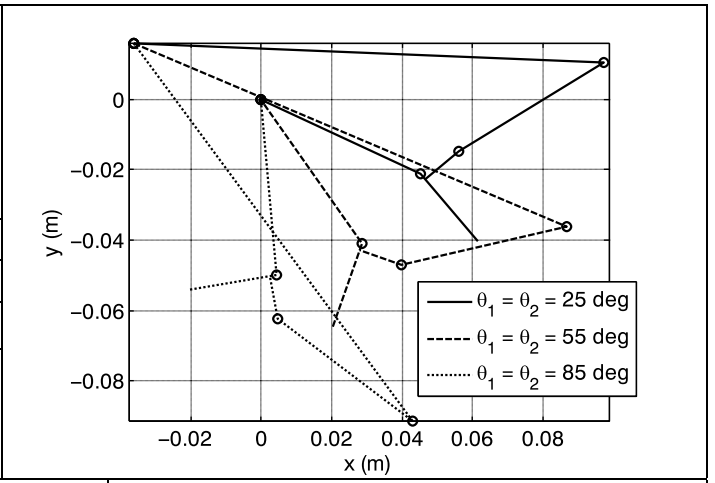
$l_{AB} = 0.1335$	
$l_{BC} = 0.0482$	
${}^2p_{O_2C} = [0.0020 \quad 0.0124]^T$	
${}^0p_{O_1A} = [-0.0362 \quad 0.0160]^T$	

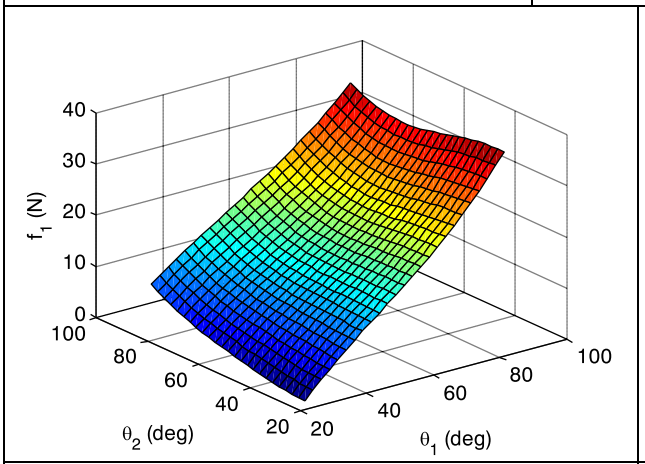

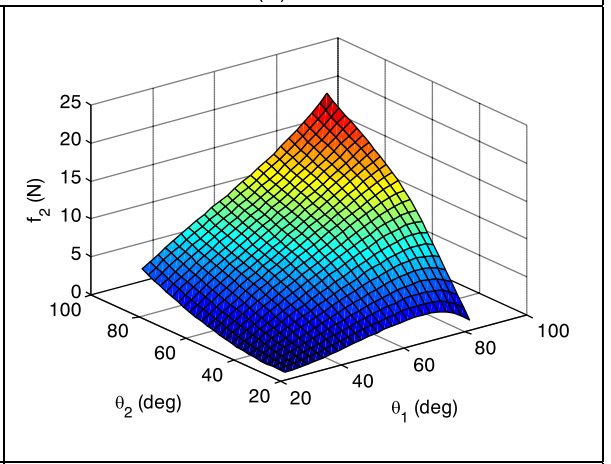

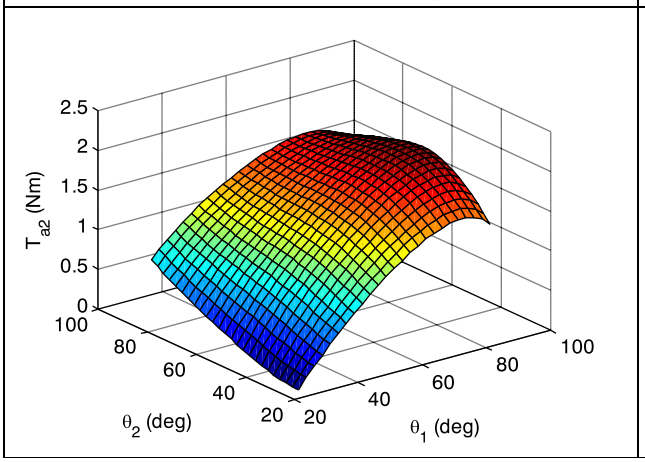

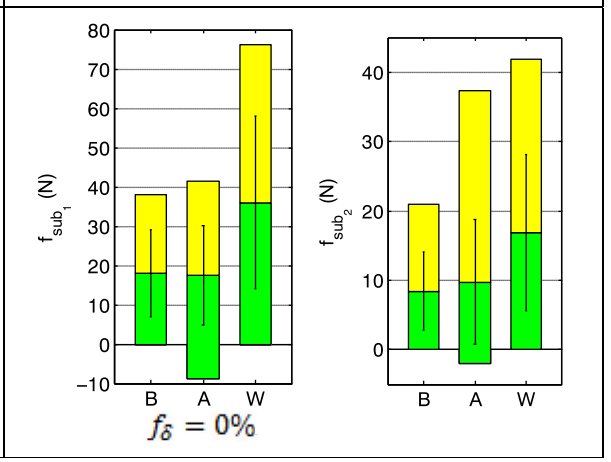

constitutes the worst case, labeled by a W). The term f_δ, defined in Eq. (19b) and expressing the percentage of the workspace where the device is not stable and the contact is not guaranteed, is also reported.

The second simulation, also dealing with Set #1 and reported in Table 3, shows the best configuration obtained when the quality of the workspace is favored with respect to its extension. In practice, the parameters are set as $p_\delta = 100$ and $p_\eta = 1$. Moreover, the workspace is considered to have some more important areas, while in other zones a decay of the device performance is not so significant. In particular, given a mean grip gesture from a hand in an extended position, the finger joints

will rotate according to preferred laws, and some finger configurations will be more common than others, from a statistical point of view. Thus, it is plain to let the device perform better along these configurations with respect to the others that are presumed to be rarely exploited by the exoskeleton. In order to take into account this fact, the γ function will be no longer constantly unitary,

Table 3
Output of the simulation: Set #1 boundaries.

$p_\delta = 1e^2$
$p_\eta = 1$

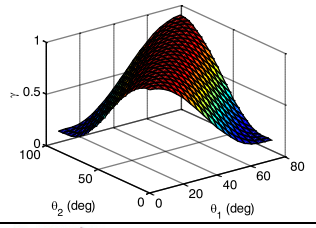

$l_{AB} = 0.1054$
$l_{BC} = 0.0131$
${}^2p_{O_2C} = [-0.0030 \quad 0.0120]^T$
${}^0p_{O_1A} = [-0.0442 \quad 0.0160]^T$

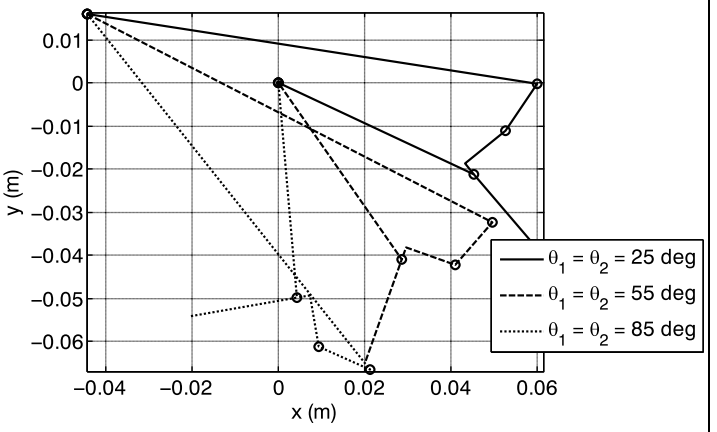

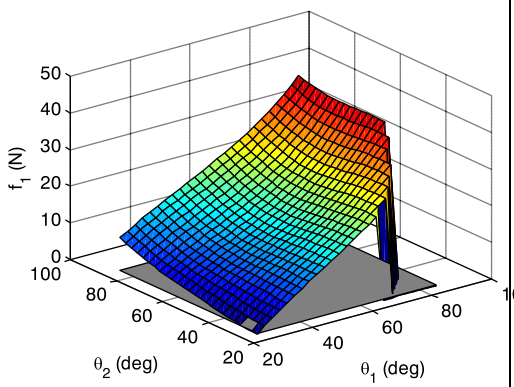

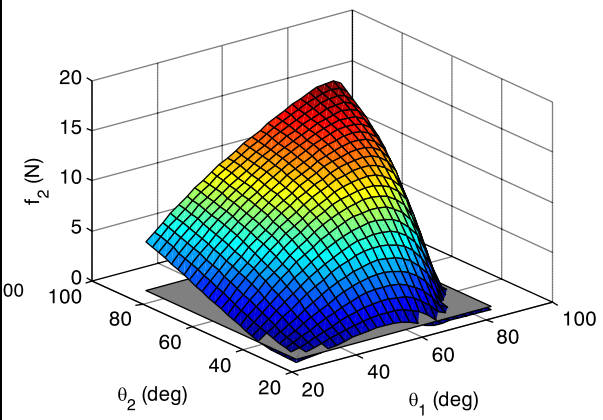

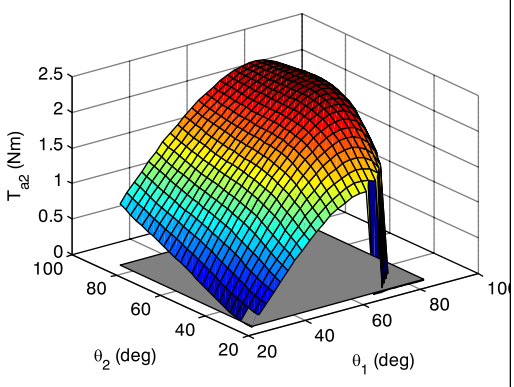

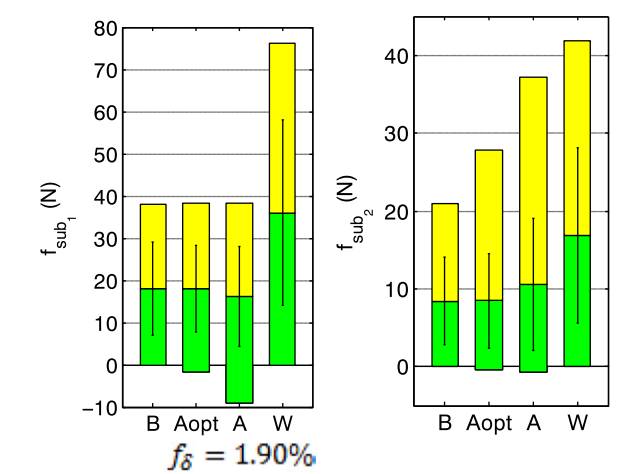

$f_\delta = 1.90\%$

but it will vary between 0 and 1. The imposed trend of γ is reported in Table 3, too. The best configuration obtained through the optimization process is effective along a vast majority of the workspace area ($f_\delta < 2\%$), and, from the point of view of the transmitted forces, it has a better performance on the area where the function γ is high with respect to the others (it is significant that the configurations where the exoskeleton fails to transmit any forces are characterized by low γ values). In particular, the

Table 4
Output of the simulation: Set #2 boundaries.

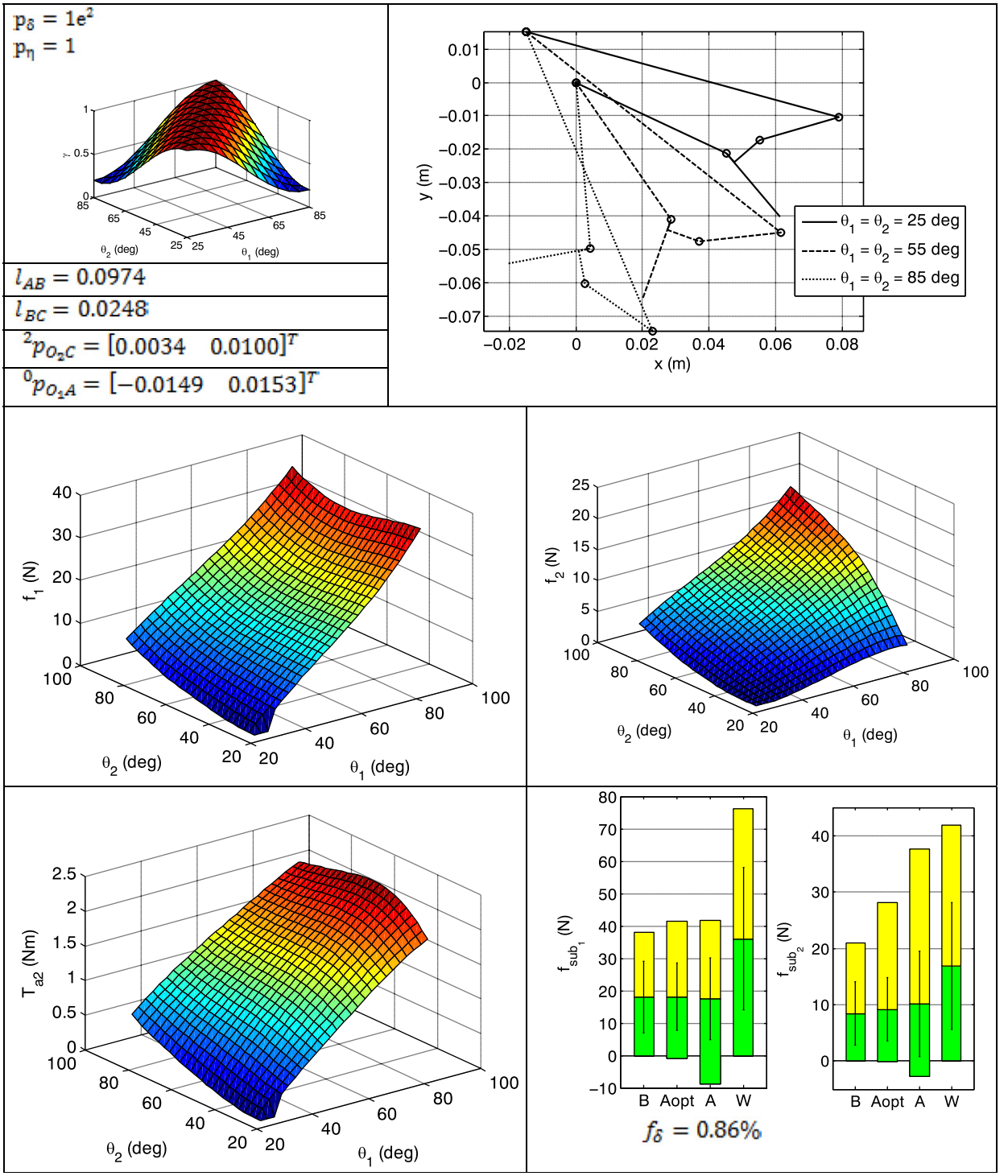

histograms reported in Table 3 show that the mean, the maximum and the minimum forces that the subject exerts on an optimal area (defined by the condition $\gamma > 0.8$ and labeled as Aopt in the picture) are more proximal to the best case B, with respect to the force distribution evaluated along the whole workspace, labeled as case A. Examining the configurations where the mechanism fails to transmit forces to the phalanges in the case shown in Table 3, the failure happens when a singularity occurs: in particular, the segments AB and *BC* become collinear, and the mechanism does not work properly. From an analytical point of view, the determinant of the matrix T, reported in Eq. (12), becomes null. In order to solve this problem, a proper joint limit stop can be introduced. The histograms of Table 3 show that the performance of the mechanism for the first phalange has a very good behavior, while the second one has a good behavior for what concerns the mean value of the force, while the maximum value is quite high. The result is better for what concerns the optimal area Aopt: even if the maximum value is 33% higher than the best case, the mean values are practically equal and the standard deviation values are within 8% of the best case. In other words, the optimization based on the γ function is able to guarantee a central area that has a performance quite similar to the best case.

Finally, Table 4 again proposes an optimization exploiting the weights of $p_\delta = 100$ and $p_\eta = 1$ and the non-constant trend of the γ function, but considering the parameter boundaries labeled as Set #2 in Table 1. With respect to the previous cases, the more demanding constraints are expected to produce a solution that constitutes a compromise: it has a lower bulk and its performance should slightly decrease. This can be seen for example for the first phalange, as now the maximum forces cross the value of 40 N, while in the previous case reported in Table 3 they were lower. However, the area where the exoskeleton fails to exert proper forces, due to singularities, is now lower.

In conclusion, the current paragraph has shown that several optimized configurations can be obtained, given the proper tuning of a number of input parameters, which can drive the simulation algorithm towards solutions that favor some aspects more than others. However, all the optimal configurations of the device have a common feature that descends from the definition

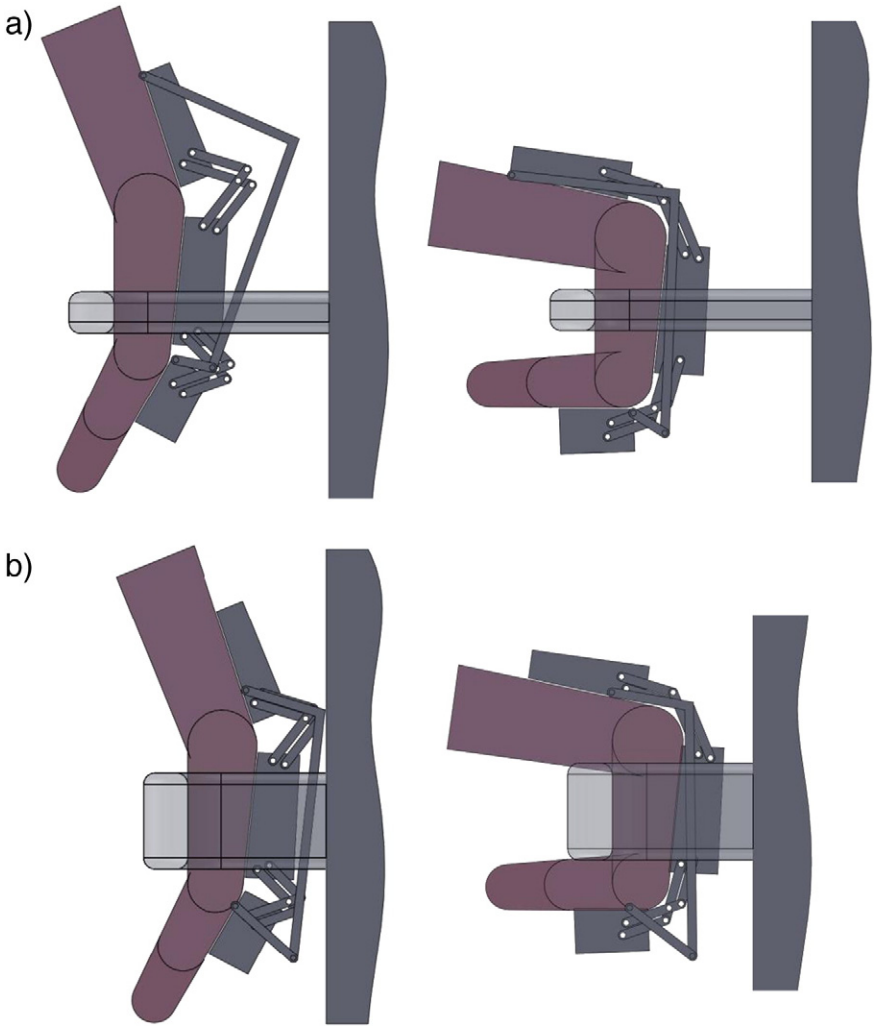

Fig. 8. Grabbing operations with the proposed exoskeletons: a) case of the tool handle, solution of Table 3; b) case of the EVA handhold, solution of Table 4.

of the glove reaction forces: they are very proximal to a singularity configuration when the finger exoskeleton is towards a complete extension. In particular, the condition where the segments *BC* and CO_2 are collinear arises here. In fact, such position of the finger is associated with a very low glove reaction force: hence, a close-to-a-singularity situation is not a big handicap. On the other side, when the rotation angles increase and the finger is flexed, the arm of the force that the transmission part exchanges with the finger-like one grows.

Finally, Fig. 8 shows how the solutions reported in Tables 3 and 4 deal with the human finger and the external constraints of EVA. In particular, the solution coming from Table 3, that permits one to grab a tool handle, is shown in Fig. 8a; on the other side, Fig. 8b reports the operation of catching the standard EVA handhold, operation that is feasible with the solution of Table 4. The same figures propose the presence of the double-parallelogram units, described in paragraph 2 and here dimensioned in order not to give any interference with the human phalanges when flexed up to the maximum angle of $\theta_i = 85°$, where i = 1,2. In Fig. 8 the *AB* bar is rendered as an L-shaped object, again in order to avoid interferences during flexion. The phalanges of the exoskeleton are instead modeled as mere trapezoidal bodies, tangent to the human phalanges: this is of course only a schematic representation, not a constructive drawing.

4. Conclusion

Underactuation is a promising field to develop a new family of hand exoskeletons, which, given their requisites of being wearable and lightweight, necessitate a maximization of the simplification of their architecture. In particular, since the underactuation concept roughly consists in having less actuators than degrees of freedom, then it is possible to diminish the number of actuators of a hand exoskeleton design, in order to reduce bulk and weight.

The current paper has examined this concept, applying the theoretical results of kinetostatic analysis, previously developed for robotic hands, to exoskeletons. Since the mathematics of the problem is strongly not linear, the current approach has exploited a stochastic algorithm to define a finger exoskeleton geometry that optimizes the defined task. In particular, EVA for astronauts has been identified as a typical field of interest for exoskeletons: the force coming from the glove phalanges has been properly measured and it constitutes the input for the optimization. An index, called the global performance index, has been defined, in order to describe quantitatively the effectiveness of the optimized solution. Finally, different possible exoskeleton geometries have been synthesized, given two alternative sets of constraints, which define the maximum allowable bulk of the device, according to specific EVA tasks.

Future works will deal with the design and experimental testing of an actual prototype of the device here proposed, described and properly optimized. Proper control strategies will be implemented, in order to apply to the system the reference torque, here theoretically computed. The comparison of the results here exposed with these actual tests will constitute the guideline for a further optimization of the architecture.

Appendix A.1

The present Appendix reports a characterization of a pressurized EVA glove. The tests have been operated through a specific test bench, reported in [26], that permits one to obtain the trend of the torque of each glove phalange with respect to the angle of rotation of the phalanges of the finger. In the current paper, a representative law of the type $f_{GL\_i} = f_{GL\_i}(\theta_i)$ has been considered, i.e. the reaction torque of each finger phalange depends only on the rotation of the phalange itself. It has been found that a polynomial third degree equation constitutes a good approximation of the experimental results. The following Table 5 shows the coefficients of the polynomial laws for the MCP and PIP phalanges, where a_q is the coefficient of the term θ_i^q. The angles are expressed in degrees.

Table 5
Coefficients of the polynomial laws expressing the stiffness of the EVA glove phalanges.

	MCP	PIP
a_3	0.00000977	0.00000568
a_2	−0.00126507	−0.00077870
a_1	0.10327994	0.04390149
a_0	−1.82999712	−0.69008759

References

[1] M. Mozaffari Foumashi, M. Troncossi, V. Parenti Castelli, State-of-the-art of hand exoskeleton systems, Internal Report, DIEM, Università di Bologna, 2011.
[2] S. Cobos, M. Ferre, M. Sanchez, J. Ortego, C. Peña, Efficient human hand kinematics for manipulation tasks, IEEE/RSJ International Conference on Intelligent Robots and Systems Acropolis Convention Center. Nice, France, September 22–26, 2008, 2008.
[3] A. Chiri, F. Giovacchini, N. Vitiello, E. Cattin, S. Roccella, F. Vecchi, M.C. Carrozza, HANDEXOS: towards an exoskeleton device for the rehabilitation of the hand, Proceedings of the 2009 IEEE/RSJ International Conference on Intelligent Robots and Systems, October 11–15, 2009, St. Louis, USA, 2009.
[4] B.L. Shields, J.A. Main, S.W. Peterson, A.M. Strauss, An anthropomorphic hand exoskeleton to prevent astronaut hand fatigue during extravehicular activities, IEEE Trans. Syst. Man Cybern. Syst. Hum. 27 (5) (1997) 668–673.

[5] M. Fontana, A. Dettori, F. Salsedo, M. Bergamasco, Mechanical design of a novel hand exoskeleton for accurate force displaying, Proceedings of the IEEE International Conference on Robotics and Automation, May 12–17, 2009, Kobe, Japan, 2009.
[6] S. Cobos, M. Ferre, M. Sanchez, J. Ortego, Constraints for realistic hand manipulation, PRESENCE 2007, The 10th Annual International Workshop on Presence, October 25–27 Barcelona, Spain, 2007, pp. 369–370.
[7] L. Birglen, C. Gosselin, T. Laliberté, Underactuated Robotic Hands, Springer, 2008.
[8] A. Bicchi, Hands for dexterous manipulation and powerful grasping: a difficult road toward simplicity, IEEE Trans. Robot. Autom. 16 (2000) 652–662.
[9] H. de Visser, J.L. Herder, Force-directed design of a voluntary closing hand prosthesis, J. Rehabil. Res. Dev. 37 (3) (2000) 261–272.
[10] S. Hirose, Y. Umetani, The development of soft gripper for the versatile robot hand, Mech. Mach. Theory 13 (1978) 351–358.
[11] M. Rakic, Multifingered robot hand with self-adaptability, Robot. Comput. Integr. Manuf. 3 (2/3) (1989) 269–276.
[12] C. Gosselin, F. Pelletier, T. Laliberte, An anthropomorphic underactuated robotic hand with 15 dofs and a single actuator, Robotics and Automation, 2008. ICRA 2008. IEEE International Conference on. IEEE, 2008, pp. 749–754.
[13] C. Brown, H. Asada, Inter-finger coordination and postural synergies in robot hands via mechanical implementation of principal components analysis, Intelligent Robots and Systems, 2007, IROS 2007. IEEE/RSJ International Conference on. IEEE, 2007, pp. 2877–2882.
[14] G. Grioli, M. Catalano, E. Silvestro, S. Tono, A. Bicchi, Adaptive synergies: an approach to the design of under-actuated robotic hands, International Conference of Intelligent Robots and Systems IROS, 2012, pp. 1251–1256.
[15] M. Mulas, M. Folgheraiter, G. Gini, An EMG-controlled exoskeleton for hand rehabilitation, Proceedings of the IEEE 9th International Conference on Rehabilitation Robotics, June 28–July 1, 2005, Chicago, IL(USA), 2005, pp. 371–374.
[16] J. Iqbal, N.G. Tsagarakis, A.E. Fiorilla, D.G. Caldwell, A portable rehabilitation device for the hand, Engineering in Medicine and Biology Society (EMBC), Annual International Conference of the IEEE, 2010, pp. 3694–3697.
[17] A. Chiri, F. Giovacchini, S. Roccella, N. Vitiello, E. Cattin, F. Vecchi, M.C. Carrozza, Handexos: Towards a Support Device for Hand Activities and Telepresence, ESTEC, Noordwijk, The Netherlands, November 11–13 2008.
[18] H. Kawasaki, S. Ito, Y. Ishigure, Y. Nishimoto, T. Aoki, T. Mouri, H. Sakaeda, M. Abe, Development of a hand motion assist robot for rehabilitation therapy by patient self-motion control, Proceedings of the IEEE 10th International Conference on Rehabilitation Robotics, June 12–15, 2007, Noordwijk, The Netherlands, 2007, pp. 234–240.
[19] C.D. Takahashi, L. Der-Yeghiaian, V.H. Le, S.C. Cramer, A robotic device for hand motor therapy after stroke, Proceedings of the IEEE 9th International Conference on Rehabilitation Robotics, June 28–July 1, 2005, Chicago, IL (USA), 2005, pp. 17–20.
[20] Rui C.V. Loureiro, W.S. Harwin, Reach & grasp therapy: design and control of a 9-DOF robotic neuro-rehabilitation system, Proceedings of the IEEE 10th International Conference on Rehabilitation Robotics, June 12–15, 2007, Noordwijk, The Netherlands, 2007, pp. 757–763.
[21] T. Laliberte, C.M. Gosselin, Simulation and design of underactuated mechanical hands, Mech. Mach. Theory 33 (1998) 39–57.
[22] L. Wu, G. Carbone, M. Ceccarelli, Designing an underactuated mechanism for a 1 active DOF finger operation, Mech. Mach. Theory 44 (2) (2009) 336–348.
[23] L. Birglen, C.M. Gosselin, Kinetostatic analysis of underactuated fingers, IEEE Trans. Robot. Autom. 20 (2) (2004) 211–221.
[24] A. Favetto, E.P. Ambrosio, S. Appendino, A. Battezzato, F. Chen Chen, D. Manfredi, M. Mousavi, F. Pescarmona, Embedding an exoskeleton hand in the astronaut's EVA glove: feasibility and ideas, Int. J. Aerosp. Sci. 1 (4) (2012).
[25] E. Mateson, G. Brooker, Augmented robotic device for EVA hand manoeuvres, Acta Astronaut. 81 (2012) 51–61.
[26] M. Mousavi, S. Appendino, A. Battezzato, F. Chen Chen, A. Favetto, F. Pescarmona, Stiffness of an EVA glove: objective evaluation and testing procedures, ASTRA, 12th Symposium on Advanced Space Technologies in Robotics and Automation, 2013.
[27] S. Kirkpatrick, C.D. Gelatt, M.P. Vecchi, Optimization by simulated annealing, Science 220 (4598) (May 13 1983) 671–680 (New Series).
[28] H. Yamaura, K. Matsushita, R. Kato, H. Yokoi, Development of hand rehabilitation system for paralysis patient — universal design using wire-driven mechanism, 31st Annual International Conference of the IEEE EMBS, September 2–6, 2009, Minneapolis, Minnesota (USA), 2009.
[29] G. Zong, X. Pei, J. Yu, S. Bi, Classification and type synthesis of 1-DOF remote center of motion mechanisms, Mech. Mach. Theory 43 (2008) 1585–1595.
[30] C.M. Gosselin, J. Angeles, Singularity analysis of closed-loop kinematic chains, robotics and automation, IEEE Trans. 6 (3) (1990).
[31] M. Welsh, D. Akin, The effects of extravehicular activity gloves on human hand performance, SAE Technical Paper, 2001, http://dx.doi.org/10.4271/2001-01-2164.
[32] J.A. Main, S.W. Peterson, A.M. Strauss, Highly mobile space suit material optimization, Acta Astronaut. 36 (1) (1995) 73–79.
[33] NASA-STD-3000 Volume 1, Man-Systems Integration Standards, 1995.